Quantitative orientation-independent differential interference contrast microscope with fast switching shear direction and bias modulation

Michael Shribak

Marine Biological Laboratory, 7 MBL St., Woods Hole, Massachusetts 02543, USA (e-mail: mshribak@mbl.edu)

Received December 21, 2012; revised February 20, 2013; accepted February 20, 2013;
posted February 22, 2013 (Doc. ID 182308); published March 27, 2013

We describe a quantitative orientation-independent differential interference contrast (DIC) microscope, which allows bias retardation to be modulated and shear directions to be switched rapidly without any mechanical movement. The shear direction is switched by a regular liquid-crystal cell sandwiched between two standard DIC prisms. Another liquid-crystal cell modulates the bias. Techniques for measuring parameters of DIC prisms and calibrating the bias are shown. Two sets of raw DIC images with the orthogonal shear directions are captured within 1 s. Then the quantitative image of optical path gradient distribution within a thin optical section is computed. The gradient data are used to obtain a quantitative distribution of the optical path, which represents the refractive index gradient or height distribution. Computing enhanced regular DIC images with any desired shear direction is also possible.

OCIS codes: 180.0180, 120.3940, 170.3890, 120.0120, 120.3180, 100.2980.

1. INTRODUCTION

A differential interference contrast (DIC) light microscope is a polarizing beam-shearing interference system in which the interfering beams are sheared by a small amount, generally by somewhat less than the radius of an Airy disk. The DIC technique produces a monochromatic shadow-cast image that displays the gradient of optical paths. Those regions of the specimen where the optical paths increase along a reference direction appear brighter (or darker), while regions where the path differences decrease appear in reverse contrast. As the gradient of the optical path grows steeper, image contrast is significantly increased. Another important feature of the DIC technique is that it produces effective optical sectioning. This is particularly obvious when high-numerical aperture (NA) objectives are used together with high-NA condenser illumination.

The DIC technique was invented by Smith in 1947 [1,2]. He placed between a pair of the crossed polarizers one Wollaston prism at the front focal plane of the condenser and another Wollaston prism at the back focal plane of the objective lens. The splitting angles of the prisms ε_1 and ε_2 are connected with the focal distances of the condenser and objective f_c and f_{ob} and the shear amount d by the following relation:

$$f_c\varepsilon_1 = f_{\mathrm{ob}}\varepsilon_2 = d. \tag{1}$$

However, in conventional medium- to high-NA objective lenses, the back focal plane is located inside the lens system and therefore is not available for insertion of a Wollaston prism. The Smith shearing DIC scheme requires special design for the microscope objective lenses so that the Wollaston prism can be incorporated within.

Nomarski, who proposed in 1952 a special polarization prism, took another approach [3,4]. He devised a prism that introduces spatial displacement and angular deviation of orthogonally polarized beams simultaneously. The Nomarski prism can therefore be placed outside of the objective lens.

The DIC microscopy demonstrates remarkable optical sectioning capability, like confocal microscopy. The contrast in DIC is produced by the optical path difference in a small in-focus volume in which two interfering beams are spatially separated. Here the beams travel through the different areas of the specimen under investigation. The out-of-focus object introduces practically the same phase disturbance in both beams because the beams go through almost the same area of the specimen. Therefore, the out-of-focus disturbance is suppressed by optical subtraction. It was shown experimentally [5] that the depth of the optical sections, with illumination at 546 nm and a 0.95 NA objective lens, could be 0.25 μm for DIC microscopy. Using formulas from [6], one can find that, with the same condition, the theoretical depth of field of the conventional bright-field microscope is 0.8 μm. The optical section depth becomes thinner if the shear amount is smaller, and the objective and condenser NAs are larger. The narrow optical sectioning DIC phenomenon is similar to removing an out-of-focus haze in the structured illumination microscopy (SIM) [6]. The SIM employs a single-spatial-frequency grid pattern, which is projected onto the object under investigation. Raw images are taken at three spatial positions of the grid. The out-of-focus picture of the object does not depend on the pattern position. As a result, the out-of-focus haze in SIM is subtracted computationally.

Application of computation subtraction in the DIC should also improve its sectioning capability even further. The

computation subtraction of images with different biases is employed in various techniques, such as polarization-modulation DIC (PM-DIC) [7,8], differential-detection DIC (D-DIC) with a polarizing beam splitter [9], phase-shifting DIC (PS-DIC) [10–12], retardation-modulation DIC (RM-DIC) [13–15], and orientation-independent DIC (OI-DIC) [16–18]. In particular, the PM-DIC removes a background contribution that is insensitive to defocus [8]. It is shown theoretically and confirmed experimentally that an RM-DIC microscope has stronger optical sectioning than a conventional DIC microscope, and the optical section depth is thinner if a Nomarski prism with smaller shear amount is used [15]. Our experiments with the OI-DIC microscope using a 100x/1.3 NA oil immersion objective lens demonstrated the optical section depth about 0.1 μm. The corresponding field depth of a bright-field microscope would be 0.5 μm.

The regular DIC microscope, however, has shortcomings: it requires proper orientation of a specimen in relation to the optical system in order to achieve the best picture, and its images are not quantitative. In order to obtain quantitative data, it is necessary to capture DIC images with orthogonal shear directions. The previous approaches [11,19–22] used mechanical rotation either of the specimen or of the DIC prism. This takes considerable time and the obtained images can be misaligned. Therefore the previous methods in the DIC microscopy were not suitable for imaging live cells. To overcome these limitations, we have designed and successfully built a new DIC microscope, which allows the bias and shear directions to be switched rapidly without mechanically rotating the specimen or the prisms [17,18]. In this system we incorporate algorithms that we have developed. The new OI-DIC technique provides quantitative orientation-independent images of phase (dry mass) and phase gradient with the highest fidelity and resolution, which cannot be obtained with any other optical microscope.

2. PRINCIPAL OPTICAL SCHEMATICS OF ORIENTATION-INDEPENDENT DIFFERENTIAL INTERFERENCE CONTRAST MICROSCOPE

A regular DIC microscope produces images, whose contrast depends on the beam-shearing direction and phase shift (bias) between the interfering beams. In order to achieve the highest contrast of a specimen under investigation, the researcher should manually rotate a microscope stage to make the shear direction parallel to the specimen's refractive index gradient, and he/she should optimize the bias by moving a DIC prism laterally or rotating a compensator [6]. The OI-DIC microscope changes the shear direction and the bias quickly and without any mechanical manipulation [17,18]. Instead of a single DIC prism, the OI-DIC scheme employs two DIC prisms with a liquid-crystal variable retarder or a liquid-crystal 90° polarization rotator in between. This combination creates a beam-shearing assembly, which allows switching the shear direction by 90° at high speed and without image misalignment. Another liquid-crystal variable retarder works as an optical phase shifter that controls the bias. In principle, instead of liquid-crystal cells, other means for changing the light polarization can be employed.

Principal optical schematics of the OI-DIC microscope for transmitted and reflected light are shown in Figs. 1 and 2,

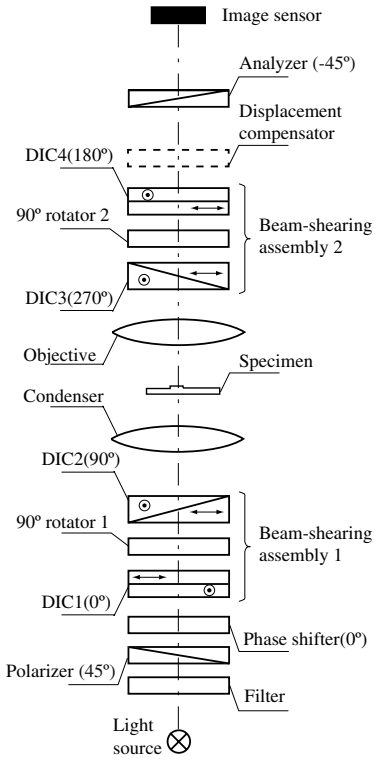

Fig. 1. Principal optical schematics of OI-DIC microscope for transmitted light.

respectively. They include a light source with a bandpath filter, a crossed linear polarizer and analyzer, a phase shifter, an objective lens, and an image sensor. The transmitted light schematic contains two beam-shearing assemblies and a condenser lens. The reflected setup has one beam-shearing assembly and a semitransparent beam splitter. Both schematics could also include a displacement compensator. Orientation of the polarizers and birefringent components is shown in the pictures. The phase shifter can be placed anywhere between the polarizers and the analyzer. It is necessary to keep

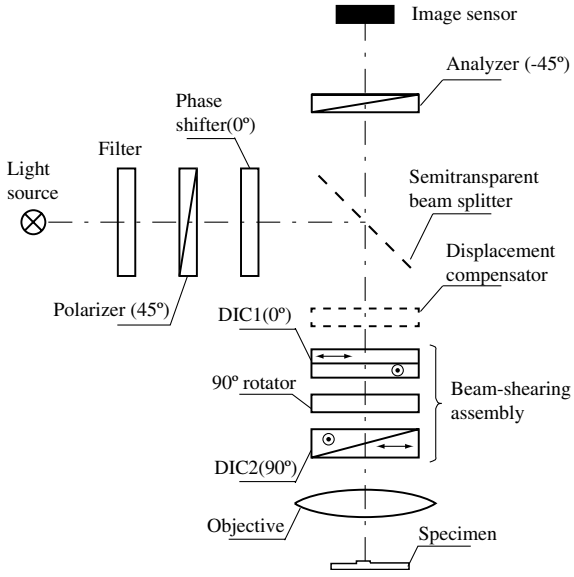

Fig. 2. Principal optical schematics of OI-DIC microscope for reflected light.

in mind that the bias will be doubled if the phase shifter is located between the beam splitter and the specimen in the reflected light scheme.

The beam-shearing assemblies could employ regular DIC prisms from the microscope. The first prism in the assembly is placed in the designed original position, and the second DIC prism is displaced along the microscope optical axis by some distance. The large prism displacement causes a strong nonuniformity of intensity distribution across the view field and reduces the image contrast significantly. One solution to the displacement problem is the using a custom-made second DIC prism, which is designed for the specific position. But this would require knowledge of the DIC prism design and such a prism could be very expensive. The second solution is to extract the bare DIC prisms from their original mounts and put them in a new holder at close distance. Thickness of each DIC prism is about 1 mm, and the thickness of a liquid-crystal cell is about 2 mm. A small displacement of the each DIC prism by 2–3 mm from the designed axial position would not deteriorate the image quality substantially. The third solution is to use the second DIC prism in its original mount and a special displacement compensator. The compensator corrects misalignment in the interfering beams caused by displacement of the prism. The axial displacement of the DIC prism changes the transversal distance between the two beams and does not change the angle between them. The compensator introduces transversal displacement in position of the extraordinary beam that is equal and opposite to the transversal distance change caused by the DIC prism. Such compensating displacement could be created by a thin calcite plane-parallel plate with the optic axis inclined at 45° to the surface, for instance. Detailed description of the compensator design is quite cumbersome, and it will be done in a future publication.

An example of the beam-shearing assembly along with the phase shifter is shown in Fig. 3 (center). The picture illustrates the polarization ray tracing in the illumination part of the transmitted light microscope (Fig. 1). Here we assume that DIC prisms are made of the positive birefringent crystal such as quartz. The diagrams to the left and right in Fig. 3 depict polarization transformations inside the assembly and the corresponding changes in the shear directions of the output beams. The left column illustrates a case when the beam polarizations between two prisms are preserved and the shear direction is 45° after the second DIC prism. The right column describes a rotation of the output shear direction by 90° caused by switching the beam polarizations after the first DIC prism.

The schematic consists of a linear polarizer **P**, a phase shifter, a pair of DIC prisms (Nomarski or Wollaston) **DIC1** and **DIC2** with orthogonal shear directions, and a 90° polarization rotator. The shear direction of the first prism **DIC1** is chosen as the initial X direction to describe the orientation of the above-mentioned optical elements. The azimuth of the transmission axis of the polarizer **P** is 45° in order to create equal intensities of polarization components that become spatially divided by the first prism.

The phase shifter introduces bias Γ between the X- and Y-polarization components. The principal axis of the phase shifter is parallel to the shear direction. Dependence of the phase retardation on the applied voltage has to be smooth enough in order to achieve the required bias change accurately and quickly. The initial bias can be adjusted by sliding

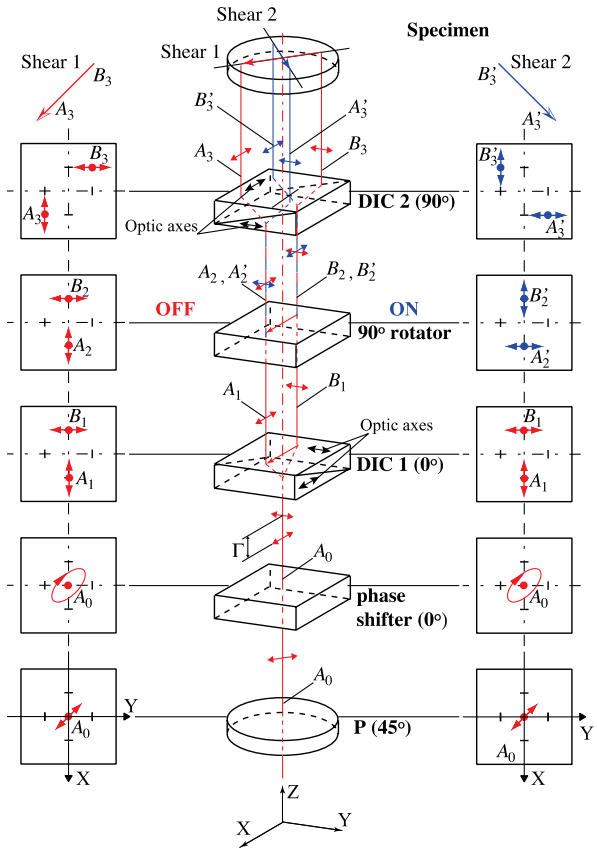

Fig. 3. (Color online) Design and principle of work of beam-shearing assembly.

the wedge component of one of the DIC prisms. In principle, the phase shifter can be installed with the same orientation in any place in the assembly. A standard untwisted nematic (TN) liquid-crystal cell, a Freedericksz cell, which works in the electrically controlled birefringence (ECB) mode [23–26], can be employed as a phase shifter. The Freedericksz cell configuration is different from the TN configuration typically used in liquid-crystal displays. Conventional Freedericksz ECB cell consists of homogeneously parallelly aligned liquid-crystal directors. The ECB mode uses the applied voltage to change the tilt of the liquid-crystal molecules; as a result, the birefringence is changed as a function of the tilt angle. When no voltage is applied, the liquid-crystal molecule's directors are aligned parallel to the cell substrates and the retardance is at a maximum. When a voltage is applied, an electric field is introduced that supplies a torque to the liquid-crystal molecules; the retardance is decreased. The molecules near the substrates are not able to fully rotate, and so the retardance does not quite get to zero. A conventional ECB cell has a retardance range from 0.1 to two waves (2λ) at 700 nm [24,25].

It is also possible to use an ECB cell with vertical alignment (VA ECB) as a phase shifter [23,27]. The liquid-crystal molecule's directors are aligned perpendicular (vertical) to the cell substrates if no voltage is applied, and the retardance is at a minimum (zero). Applied voltage turns the liquid-crystal directors, and so the retardance is increased. The vertically aligned LC cell exhibits the highest contrast value among all LC cells. Another merit is its fast response speed due to its thin cell gap. It does not require a compensation film in order to get zero retardance. The VA ECB has some shortcomings, such as a

lower retardance range from 0 to half-wave ($\lambda/2$) at 700 nm, and reduced contrast for off-axis rays.

Opposite to the phase shifter, which changes birefringence smoothly in order to obtain the required bias value, the polarization rotator has two states only. In the OFF state the beam passes through the rotator without modifying the X- and Y- polarization components. In the ON state the polarization rotator switches the X and Y components. The rotator can utilize a conventional ECB or VA ECB liquid-crystal cell, which is similar to one used by the phase shifter. In this case the principal axis of the LC cell has to be orientated at 45°. The LC cell switches polarization by 90° (ON state) when the plate retardation is half-wave ($\lambda/2$), and preserves beam polarization (OFF state) if the plate retardance is 0 or full wave (λ).

It is convenient to utilize a 90° TN cell as the rotator [26,27]. Currently the TN cells are commonly used in liquid-crystal displays and shutters. They are not expensive and are less sensitive to the wavelength variation than ECB cells. In the TN cells the LC anchoring (or rubbing) direction at the input surface is perpendicular to that of the output surface. In the inactivated state (voltage is below threshold), the local LC director undergoes a continuous twist of 90° in the region between the plates. Linearly polarized input light propagates through and, under ideal circumstances, follows the director helix as it propagates through the LC structure. Lets us assume that the LC anchoring direction at the input surface is oriented along the X axis and the anchoring direction at the output surface is oriented along the Y axis. In this case, light with initial X polarization emerges from the LC cell with Y polarization, and light with initial Y polarization comes out with X polarization. In order to reduce interaction between X- and Y- polarization components during propagation, the cell's rubbing direction should be oriented at 0° or 90°. The phase shifter could compensate a possible phase shift between two polarization components introduced by the rotator. When an electric field is applied across the LC layer, the directors become predominantly parallel to the electric field. The twisted structure is thus distorted, and, with voltage above threshold, begins to vanish. The polarization direction of the light is no longer rotated as light passes through the cell.

fast switching speed and bistability. The switching speed is very fast—usually a few microseconds. The two states are bistable, which means the electric field is not required once the tilting is finished [25,26].

Let us examine in more detail how the beam-shearing assembly works. For example, the initial ray A_0 falling on the first prism **DIC1** has coordinates (0, 0). Here the first number means a coordinate along the X axis, and the second one is the coordinate along the Y axis. The shear plane of the first DIC prism is parallel to the X axis. The prism deflects a ray with Y polarization in the negative direction by distance $-d/2$ and shifts a ray with X polarization in the positive direction by the same amount. It creates a shear distance d between the components along the X axis. Thus, the first output ray A_1 has X polarization and coordinates $(d/2, 0)$. The Y-polarized second ray B_1 has coordinates $(-d/2, 0)$.

The 90° polarization rotator preserves the linear polarizations of the beams A_1 and B_1 (OFF state) or turns them by 90° without altering the ray positions (ON state). In the first case (left column), the output rays A_2 and B_2 are polarized along the X axis and the Y axis, respectively. In the second case (right column), the rays A_2' and B_2' are polarized along the Y axis and the X axis, respectively.

The second prism **DIC2** is oriented orthogonal to the direction of the first prism. So, the shear direction of the second prism lies along the Y axis. The prism moves the position of a ray with Y polarization by distance $d/2$ in the positive direction and deflects a ray with X polarization in the negative direction by the same amount.

First we consider a case, which is shown on the left side of Fig. 3, where the rotator state is **OFF**, and therefore the ray polarizations are not changed. Then ray A_2 with X polarization and coordinates $(d/2, 0)$ passes the second prism with negative displacement $-d/2$ in the Y direction, and the output ray A_3 has coordinates $(d/2, -d/2)$. Meanwhile, the coordinates of ray B_2 are changed by $d/2$ in the positive direction along the Y axis, and the coordinates for output ray B_3 are $(-d/2, d/2)$. As a result, in the first case the dual beam that falls on the specimen has shear direction −45°. The first case can be described by the following flow chart:

$$\left|\begin{matrix}A_0(0,0)\\(E_x,E_y)\end{matrix}\right| \rightarrow \begin{cases} \boxed{\begin{matrix}\text{DIC1}\\ x\text{-shear}\end{matrix}} \rightarrow \left|\begin{matrix}A_1\left(\frac{d}{2},0\right)\\(E_x,0)\end{matrix}\right| \rightarrow \boxed{\begin{matrix}\text{rotator}\\ \textbf{OFF}\end{matrix}} \rightarrow \left|\begin{matrix}A_2\left(\frac{d}{2},0\right)\\(E_x,0)\end{matrix}\right| \rightarrow \boxed{\begin{matrix}\text{DIC2}\\ y\text{-shear}\end{matrix}} \rightarrow \left|\begin{matrix}A_3\left(\frac{d}{2},\frac{-d}{2}\right)\\(E_x,0)\end{matrix}\right| \\ \boxed{\begin{matrix}\text{DIC1}\\ x-\text{shear}\end{matrix}} \rightarrow \left|\begin{matrix}B_1\left(\frac{-d}{2},0\right)\\(0,E_y)\end{matrix}\right| \rightarrow \boxed{\begin{matrix}\text{rotator}\\ \textbf{OFF}\end{matrix}} \rightarrow \left|\begin{matrix}B_2\left(\frac{-d}{2},0\right)\\(0,E_y)\end{matrix}\right| \rightarrow \boxed{\begin{matrix}\text{DIC2}\\ y\text{-shear}\end{matrix}} \rightarrow \left|\begin{matrix}B_3\left(\frac{-d}{2},\frac{d}{2}\right)\\(0,E_y)\end{matrix}\right| \end{cases},$$

One of advantages of using the TN cell is that we do not need to know precise dependence of parameters of the cell on the applied voltage. In the transmitted light with use of two rotators we can apply the same voltage to both cells simultaneously using the same generator output. Typically the Freedericksz voltage threshold occurs at 2–3 V_{rms}. In this case, the voltage ~0.5 V_{rms} will set both rotators in the ON state, and voltage 5 V_{rms} will put them in the OFF state.

It is promising to employ a ferroelectric liquid-crystal (FLC) cell in the 90° polarization rotator. They are known for their

where E_x and E_y are the corresponding amplitudes of polarization components.

For the second case, after the rotator switches the polarizations by 90°, the ray A_2' is linearly polarized along the Y axis. Therefore the second prism **DIC2** changes the Y coordinate of the ray by $d/2$, and the output ray A_3' has coordinates $(d/2, d/2)$. Also the second prism deflects the X-polarized ray B_2' by $-d/2$, so that the second output ray B_3' has coordinates $(d/2, -d/2)$. Hence, the output beam has a shear direction +45°". This case can be illustrated by the next flow chart:

$$\left|\begin{matrix}A_0(0,0)\\(E_x,E_y)\end{matrix}\right| \rightarrow \begin{cases} \boxed{\begin{matrix}\text{DIC1}\\ x\text{-shear}\end{matrix}} \rightarrow \left|\begin{matrix}A_1\left(\frac{d}{2},0\right)\\(E_x,0)\end{matrix}\right| \rightarrow \boxed{\begin{matrix}\text{rotator}\\ \textbf{ON}\end{matrix}} \rightarrow \left|\begin{matrix}A_2'\left(\frac{d}{2},0\right)\\(0,E_y)\end{matrix}\right| \rightarrow \boxed{\begin{matrix}\text{DIC2}\\ y\text{-shear}\end{matrix}} \rightarrow \left|\begin{matrix}A_3'\left(\frac{d}{2},\frac{d}{2}\right)\\(0,E_y)\end{matrix}\right| \\ \boxed{\begin{matrix}\text{DIC1}\\ x\text{-shear}\end{matrix}} \rightarrow \left|\begin{matrix}B_1\left(\frac{-d}{2},0\right)\\(0,E_y)\end{matrix}\right| \rightarrow \boxed{\begin{matrix}\text{rotator}\\ \textbf{ON}\end{matrix}} \rightarrow \left|\begin{matrix}B_2'\left(\frac{-d}{2},0\right)\\(E_x,0)\end{matrix}\right| \rightarrow \boxed{\begin{matrix}\text{DIC2}\\ y\text{-shear}\end{matrix}} \rightarrow \left|\begin{matrix}B_3'\left(\frac{-d}{2},\frac{-d}{2}\right)\\(E_x,0)\end{matrix}\right| \end{cases}.$$

As one can see, both outcome shears have the same amount, which equals to the shear d introduced by a single DIC prism multiplied by $\sqrt{2}$. The shear vectors are mutually orthogonal and oriented at azimuths $\pm 45°$. The median axis of two beams passes through point (0, 0) in both cases. Therefore there is no misalignment between the images.

It is necessary to mention that switching the light polarization between the two DIC prisms affects the outcome bias (Fig. 3). Let us assume that prisms **DIC1** and **DIC2** introduce optical path differences Λ_1 and Λ_2 between beam components polarized parallel and perpendicular to the prism shear plane, respectively. If the rotator state is **OFF**, then polarization of ray A_1A_3 is parallel to the shear plane of the first DIC prism and perpendicular to the shear plane of the second prism. Thus, in the **OFF** state the beam-shearing assembly introduces combined bias $\Lambda_1 - \Lambda_2$. In the **ON** state the rotator switches polarizations by 90°, and the polarization of ray A_1A_3' is parallel to the shear planes of both DIC prisms. In this case the combined bias is $\Lambda_1 + \Lambda_2$.

3. DATA PROCESSING

A. Mathematical Model of OI-DIC Image

A conventional DIC image can be modeled as the superposition of one image over an identical copy that is displaced in the object (specimen) plane by a small shear vector **d** and phase shifted by bias Λ produced by two DIC prisms, which are located in the illumination and imaging beams, respectively. For simplicity, let us consider a phase nonbirefringent specimen with two-dimensional distribution of optical path $\phi(x,y)$. Here we use Cartesian coordinates XOY in the object plane. The specimen is illuminated by monochromatic light with wavelength λ. Intensity distribution $I(x,y)$ in the DIC image depends on the specimen orientation and varies proportionally with the scalar product of shear and optical path gradient vectors:

$$I(x,y) = \tilde{I}\sin^2\left\{\frac{\pi}{\lambda}[\Lambda + \mathbf{d}\cdot\nabla\phi(x,y)]\right\} + I_c(x,y), \quad (2)$$

where $\tilde{I}$ is the initial beam intensity, $\nabla\phi(x,y)$ is the optical path gradient vector, and $I_c(x,y)$ corresponds to an offset of the intensity signal, which is caused by the stray light.

It follows from formula (2) that if the shear and optical path gradient vectors are parallel, then their scalar product is maximal and the image contrast is maximal also. Where the shear vector is perpendicular to the gradient vector, their scalar product is zero and the contrast equals zero correspondently. Thus regular DIC technique shows two-dimensional distribution of the optical path gradient encountered along the shear direction. It is therefore prudent to examine unknown objects at several azimuth orientations.

If the X coordinate is parallel to the shear plane, then shear vector **d** and gradient vector $\nabla\phi(x,y)$ could be presented in the expanded coordinate forms:

$$\mathbf{d} = (d,0), \quad (3)$$

where d is the shear amount, and

$$\nabla\phi(x,y) \equiv \left(\frac{d\phi(x,y)}{dx}, \frac{d\phi(x,y)}{dy}\right) = (\gamma(x,y)\cos\theta(x,y), \gamma(x,y)\sin\theta(x,y)), \quad (4)$$

where $\gamma(x,y)$ is the gradient magnitude and $\theta(x,y)$ is the gradient azimuth. The gradient magnitude can be interpreted as the product of the refractive index gradient and the optical section depth.

After scalar multiplication of the shear and gradient vectors, we obtain the following equation in coordinate form for the regular DIC image:

$$I(x,y) = \tilde{I}\sin^2\left\{\frac{\pi}{\lambda}[\Lambda + d\cdot\gamma(x,y)\cos\theta(x,y)]\right\} + I_c(x,y). \quad (5)$$

As shown in Section 2, the OI-DIC beam-shearing assembly produces two orthogonal shears with shear amount equal to the shear introduced by a single DIC prism multiplied by $\sqrt{2}$. If the X coordinate is parallel to the shear plane of the first DIC prism (see Fig. 3), then shear vectors $\mathbf{d}_i$ could be written in the following coordinate form:

$$\mathbf{d}_i = (d, (-1)^i d), \quad (6)$$

where $i = 1, 2$ corresponds to the OFF or ON states of the 90° polarization rotator (first or second state of shear direction).

Another peculiarity of the OI-DIC beam-shearing assembly is that the bias introduced by its internal DIC prism is subtracted when the polarization rotator is in the OFF state or it is are added when the polarization rotator is in the ON state. In case of the transmitted light microscope (Fig. 1), the combined bias $\Lambda_{\Sigma i}$ would be determined by the formula

$$\Lambda_{\Sigma i} = \Lambda_1 + \Lambda_4 + (-1)^i(\Lambda_2 + \Lambda_3), \quad (7)$$

where Λ_1, Λ_2, Λ_3, and Λ_4 are biases contributed by prisms DIC1, DIC2, DIC3, and DIC4, respectively.

The combined bias of the reflected light setup (Fig. 2) is described by a similar equation:

$$\Lambda_{\Sigma i} = 2\Lambda_1 + (-1)^i\Lambda_2. \quad (8)$$

Substituting Eqs. (4) and (6) into Eq. (2), and taking into account variable bias Γ created by the phase shifter and combined bias $\Lambda_{\Sigma i}$ introduced by DIC prisms [see formulae (7) and (8)], we readily find the equation describing the OI-DIC microscope:

$$I_i(x,y)=\tilde{I}\sin^2\left\{\frac{\pi}{\lambda}\left[\Gamma+\Lambda_{\Sigma i}+\sqrt{2}d\cdot\gamma(x,y)\cos\left(\theta(x,y)-(-1)^i\frac{\pi}{4}\right)\right]\right\}+I_c(x,y), \quad (9)$$

where note $i=1,2$ corresponds to the first or second state of shear direction, $-45°$ or $+45°$, respectively.

B. Optimal Bias

In order to achieve the best DIC picture it is necessary to apply the optimal bias. For example, we have an extremely shallow depression or elevation that introduces a small optical path difference between the studied structure and the media. The high bias would create a bright background and the observed structure would be hardly visible. If bias is low the image background field becomes dark gray and yields very high sensitivity, bringing out image regions with minute phase differences. This conclusion is in agreement with data obtained by Salmon and Tran [28], who indicate that the best contrast is achieved when bias is adjusted to extinguish the light coming from one edge of the object of interest. This occurs when bias equals the optical path difference introduced by the edge with the opposite sign. Salmon and Tran found that for the edges of organelles and cells, the optical path difference corresponds to about $\lambda/10$th the wavelength or greater, but for microtubules and tiny organelles in the cell, the optical path difference is very small, less than 1/100th of the wavelength of green light. They recommend using about 1/15th–1/20th of the wavelength bias for observation of microtubules in order to have sufficient light at the camera. A similar result was found by Schnapp [29].

The bias optimization can be explored using Eq. (5). Let us consider a simplified sample with a binary gradient magnitude distribution such that half of the sample has a gradient magnitude of $+\gamma$ and the other half has a phase difference of $-\gamma$. The shear and gradient directions of the sample are parallel ($\theta=0°$).

We expect the best results to be achieved when DIC images have the highest contrast C:

$$C=\frac{I_{\max}-I_{\min}}{I_{\max}+I_{\min}}, \quad (10)$$

where $I_{\max}$ and $I_{\min}$ are the maximal and minimal intensities in the image.

The maximal and minimal intensities can be determined using Eq. (5). For the specimen under consideration, the contrast of DIC image is the following:

$$C=\frac{\sin\left(\frac{2\pi}{\lambda}\Lambda\right)\sin\left(\frac{2\pi}{\lambda}\gamma d\right)}{1-\cos\left(\frac{2\pi}{\lambda}\Lambda\right)\cos\left(\frac{2\pi}{\lambda}\gamma d\right)+\frac{2I_c}{\tilde{I}}}. \quad (11)$$

The ratio $I_c/\tilde{I}$ is called the extinction ratio. Derivative $dC/d\Lambda$ of this equation is the following:

$$\frac{dC}{d\Lambda}=\sin\left(\frac{2\pi}{\lambda}\gamma d\right)\frac{\left(1+\frac{2I_c}{\tilde{I}}\right)\cos\left(\frac{2\pi}{\lambda}\Lambda\right)-\cos\left(\frac{2\pi}{\lambda}\gamma d\right)}{1-\cos\left(\frac{2\pi}{\lambda}\Lambda\right)\cos\left(\frac{2\pi}{\lambda}\gamma d\right)+\frac{2I_c}{\tilde{I}}}. \quad (12)$$

The derivative is zero at $\Lambda\approx\gamma\cdot d$. Thus, the maximal contrast is achieved when bias equals the optical path difference in the sample.

According to formula (11), the contrast of microtubules and tiny organelles with phase difference $\lambda/100$ equals 0.38 at bias $\lambda/20$, and the stray light in the system is absent; it equals 0.27 at bias $\lambda/20$ and extinction ratio 100, and it equals 0.06 at bias $\lambda/4$ with both extinctions. The contrast at the small bias is more six times the one at the large bias. But it is very important to have a high extinction in order to effectively use a small bias for studying tiny structures. The contrast of cell walls and organelle edges with phase difference $\lambda/10$ is 0.79 at bias $\lambda/20$ and infinity extinction, 0.72 at bias $\lambda/20$ and extinction 100, and 0.59 at bias $\lambda/4$ and both extinctions.

In addition to reducing contrast, the low extinction decreases the dynamic range of measurement and can cause a diffraction anomaly in the Airy pattern. The lower extinction is a significant problem in microscopes equipped with high-NA lenses. To reduce the beam depolarization, we can use a polarization rectifier [30,31].

C. Algorithm for Mapping Two-Dimensional Gradient Vector Field Using Low Bias Swing

The contrast in a DIC image is generated in a very thin optical section of the specimen. The estimated thickness of the section could be about a few tenths of micrometers in the case of employing a high-NA objective lens. Additional contrast reduction occurs if the high-resolution DIC prisms with small shear amount are exploited. Taking into account that the maximal difference between refractive indices of cell structures and surrounding water media is 0.2, the maximal optical path difference would be about 0.1 μm for most biological specimens. This number corresponds to 1/5th the wavelength of green light. Actually, in most cases, the introduced optical path difference is significantly less than that. Therefore it would be beneficial to use a low bias for obtaining the best pictures.

This approach requires preliminary alignment of the OI-DIC system in order to work near the light extinction. At first, it is necessary to set the internal DIC prisms in such a position that they mutually compensate or do not introduce the bias, $\Lambda_2+\Lambda_3=0$ or $\Lambda_2=0$ [see formulas (7) and (8), respectively]. This allows us to eliminate the bias that depends on shear direction. Next, using the external DIC prisms and/or the phase shifter, we have to achieve the darkest background in the image. That means the total bias is zero, $\Gamma+\Lambda_\Sigma=0$.

In order to find the two-dimensional distribution of the gradient magnitude and azimuth γ and θ, we capture two sets of raw DIC images at shear directions $-45°$ and $+45°$ with negative, zero, and positive biases: $-\Gamma_0$, 0, and $+\Gamma_0$ [18]. The following group of equations represents these six DIC images:

$$I_{ij}(x,y)=\tilde{I}\sin^2\left\{\frac{\pi}{\lambda}\left[j\Gamma_0+\sqrt{2}d\gamma(x,y)\cos\left(\theta(x,y)-(-1)^i\frac{\pi}{4}\right)\right]\right\}+I_c(x,y), \quad (13)$$

where $j=-1,0,1$.

Initially two terms are computed ($i=1,2$):

$$A_i(x,y)=\frac{I_{i,1}(x,y)-I_{i,-1}(x,y)}{I_{i,1}(x,y)+I_{i,-1}(x,y)-2I_{i,0}(x,y)}\tan\left(\frac{\pi\Gamma_0}{\lambda}\right). \quad (14)$$

Using Eq. (13), we can show that

$$A_1(x,y) = \tan\left(\frac{2\sqrt{2}\pi}{\lambda} d\gamma(x,y)\cos\left(\theta(x,y)+\frac{\pi}{4}\right)\right),$$
$$A_2(x,y) = \tan\left(\frac{2\sqrt{2}\pi}{\lambda} d\gamma(x,y)\sin\left(\theta(x,y)+\frac{\pi}{4}\right)\right). \quad (15)$$

Using the obtained terms, we can calculate the quantitative two-dimensional distributions of the gradient magnitude and azimuth of optical paths in the specimen as

$$\gamma(x,y) = \frac{\lambda}{2\sqrt{2}\pi d}\sqrt{\sum_{i=1}^{2}\arctan^2[A_i(x,y)]},$$
$$\theta(x,y) = \arctan\left(\frac{\arctan A_2(x,y)}{\arctan A_1(x,y)}\right) - \frac{\pi}{4}. \quad (16)$$

The gradient magnitude represents the increment of the optical path difference, which is in nanometers, along the lateral coordinate, which is also in nanometers. Thus, the gradient magnitude is unitless. The shear amount d can be measured as it is described in Appendix A or found in Table 1.

Notice that the algorithm considered above employs ratios between intensities of light that have interacted with the specimen. Therefore it suppresses contributions of absorption by the specimen or from nonuniformity of illumination, which can otherwise deteriorate a DIC image.

D. Algorithm for Mapping Two-Dimensional Gradient Vector Field Using $\pi/4$ Phase Step

If the maximal optical path difference exceeds 1/5th the wavelength, we can also employ other algorithms, which are similar to the one used in phase-shifting interferometers [32]. For example, let us consider the modification of the algorithm using four frames of intensity data recorded with phase shifts of 0, $\pi/2$, π, and $3\pi/2$. This algorithm is common in the interference microscopy [6]. We proposed a similar approach for mapping birefringence at normal reflection [33].

Under these conditions, the intensity distribution $I_{ij}(x,y)$ on the CCD camera is

$$I_{i,j}(x,y) = \tilde{I}\sin^2\left\{\frac{j\pi}{4} + \frac{\sqrt{2}\pi d\gamma(x,y)}{\lambda}\cos\left(\theta(x,y) - (-1)^i\frac{\pi}{4}\right)\right\} + I_c(x,y), \quad (17)$$

where $j = 0, 1, 2, 3$ conforms to four biases, and $i = 1, 2$ corresponds to the OFF and ON states of the polarization rotators. Here we took into account that phase step $\pi/2$ is created by bias step $\lambda/4$.

Next, two terms are calculated:

$$\tilde{A}_i(x,y) = \frac{I_{i,3}(x,y) - I_{i,1}(x,y)}{I_{i,0}(x,y) - I_{i,2}(x,y)}. \quad (18)$$

Using Eq. (17), we have

$$\tilde{A}_1(x,y) = \tan\left(\frac{2\sqrt{2}\pi}{\lambda} d\gamma(x,y)\cos\left(\theta(x,y)+\frac{\pi}{4}\right)\right),$$
$$\tilde{A}_2(x,y) = \tan\left(\frac{2\sqrt{2}\pi}{\lambda} d\gamma(x,y)\sin\left(\theta(x,y)+\frac{\pi}{4}\right)\right). \quad (19)$$

Finally we obtain the quantitative two-dimensional distributions of the gradient magnitude and the azimuth of the optical paths:

$$\gamma(x,y) = \frac{\lambda}{2\sqrt{2}\pi d}\sqrt{\sum_{i=1}^{2}\arctan^2[\tilde{A}_i(x,y)]},$$
$$\theta(x,y) = \arctan\left(\frac{\arctan \tilde{A}_2(x,y)}{\arctan \tilde{A}_1(x,y)}\right) - \frac{\pi}{4}. \quad (20)$$

The choice of the algorithms with low bias swing or $\pi/4$ step depends on the optical path difference range of the specimen under investigation. The first algorithm is more sensitive for the specimen with low optical path difference. It could be optimized to get the best picture by using swing that equals the maximal optical path difference. The second algorithm does not require preliminary estimation of the optical path difference range. It works well with large optical path differences. The researcher could start with the second algorithm in order to estimate the specimen optical path difference and then apply the first algorithm with an optimized swing amount.

E. Correction of Background Gradient Vector Field

When measuring a specimen with small gradient magnitude, it is important to minimize errors that are due to the background gradient vector field across the image. Lenses, DIC prisms, LC rotators, and phase shifters contribute to the background. The spatially varying background gradient vector field leads to systematic error in the measurement of specimen gradient magnitude and azimuth.

For correction of the background gradient vector field, it is possible to employ a special procedure, whose mathematical description we published early [34,35]. The procedure is based on specimen images, which are recorded with no structures in the optical path. In order to record the background set of images, the object is moved out of the camera view field by use of the x–y translator of the microscope. If empty area

Table 1. Measured Shear Angles, and Computed Shear Distances and Ratios of Shear Distance to Airy Disk Radius for Various Combinations of Olympus DIC Prisms and Objective Lenses at Wavelength 532 nm

		Shear Distance, d (top); and Ratio d/r_{Airy} (bottom)						
DIC Prism Type	Shear Angle, ε	UplanFl 10x/0.30	UplanFl 20x/0.50	UplanSApo 30x/1.05 Sil	UplanFl 40x/0.75	UplanSApo 60x/1.20 W	UplanSApo 60x/1.30 Sil	UplanFl 100x/1.30 Oil
U-DICTHR	39 μrad	0.70 μm; 0.65	0.35 μm; 0.54	0.23 μm; 0.76	0.18 μm; 0.40	0.12 μm; 0.43	0.12 μm; 0.47	0.07 μm; 0.28
U-DICT	75 μrad	1.35 μm; 1.25	0.67 μm; 1.04	0.45 μm; 1.46	0.34 μm; 0.78	0.22 μm; 0.83	0.22 μm; 0.90	0.14 μm; 0.54
U-DICTHC	149 μrad	2.68 μm; 2.48	1.34 μm; 2.07	0.89 μm; 2.89	0.67 μm; 1.55	0.45 μm; 1.65	0.45 μm; 1.79	0.27 μm; 1.07

around the object is not available, one could utilize a defocused picture of the object as the background. The background images are captured at the same beam-shearing assembly settings as for the object itself. Using these images, we compute terms $A_{bgi}(x,y)$ or $\tilde{A}_{bgi}(x,y)$ according to formulae (14) or (18). Then the differences between the terms $A_i(x,y) - A_{bgi}(x,y)$ or $\tilde{A}_i(x,y) - \tilde{A}_{bgi}(x,y)$ are used in modified formulas (16) or (20) for determining gradient magnitude and azimuth:

$$\gamma(x,y) = \frac{\lambda}{2\sqrt{2}\pi d}\sqrt{\sum_{i=1}^{2}\arctan^2[A_i(x,y) - A_{bgi}(x,y)]},$$
$$\theta(x,y) = \arctan\left(\frac{\arctan[A_2(x,y) - A_{bg2}(x,y)]}{\arctan[A_1(x,y) - A_{bg1}(x,y)]}\right) - \frac{\pi}{4}, \quad (21)$$

or

$$\gamma(x,y) = \frac{\lambda}{2\sqrt{2}\pi d}\sqrt{\sum_{i=1}^{2}\arctan^2[\tilde{A}_i(x,y) - \tilde{A}_{bgi}(x,y)]},$$
$$\theta(x,y) = \arctan\left(\frac{\arctan[\tilde{A}_2(x,y) - \tilde{A}_{bg2}(x,y)]}{\arctan[\tilde{A}_1(x,y) - \tilde{A}_{bg1}(x,y)]}\right) - \frac{\pi}{4}. \quad (22)$$

In addition to correcting the background gradient field of the specimen under investigation, this procedure also accounts for slight miscalibration of the polarization states of the beam-shearing assemblies.

Typically, the background retardance does not change considerably over a time period of many minutes. Therefore the intermediate results $A_{bgi}(x,y)$ or $\tilde{A}_{bgi}(x,y)$ can be employed repeatedly to correct, e.g., a time series of images measuring the subtle changes in the optical path gradient in a live specimen.

It is possible that the intensity of the illumination would fluctuate during the time series image acquisition. We observed such fluctuations using high-power mercury arc lamps. Also, retardance of the LC phase shifter could slightly vary because of a temperature change. These reasons for an error in the measured specimen gradient vector distribution cannot be corrected with the described background correction procedure. But this small error gradient would be uniform across the image. Therefore if there is an image area with known gradient vector, we can use it for additional correction.

For example, the obtained image shows some gradient magnitude γ_{cor} and azimuth θ_{cor} in an image point where the gradient is expected to be zero. This allows us to compute the correction terms $A_{\mathrm{cor}i}$ or $\tilde{A}_{\mathrm{cor}i}$, where $i = 1, 2$, using Eqs. (15) or (19), respectively:

$$A_{\mathrm{cor1}} = \tilde{A}_{\mathrm{cor1}} = \tan\left(\frac{2\sqrt{2}\pi}{\lambda} d\gamma_{\mathrm{cor}} \cos\left(\theta_{\mathrm{cor}} + \frac{\pi}{4}\right)\right),$$
$$A_{\mathrm{cor2}} = \tilde{A}_{\mathrm{cor2}} = \tan\left(\frac{2\sqrt{2}\pi}{\lambda} d\gamma_{\mathrm{cor}} \sin\left(\theta_{\mathrm{cor}} + \frac{\pi}{4}\right)\right). \quad (23)$$

Then the obtained terms are applied for calculating the corrected gradient magnitude and azimuth for the entire image:

$$\gamma(x,y) = \frac{\lambda}{2\sqrt{2}\pi d}\sqrt{\sum_{i=1}^{2}\arctan^2[A_i(x,y) - A_{bgi}(x,y) - A_{\mathrm{cor}i}]},$$
$$\theta(x,y) = \arctan\left(\frac{\arctan[A_2(x,y) - A_{bg2}(x,y) - A_{\mathrm{cor2}}]}{\arctan[A_1(x,y) - A_{bg1}(x,y) - A_{\mathrm{cor1}}]}\right) - \frac{\pi}{4}, \quad (24)$$

or

$$\gamma(x,y) = \frac{\lambda}{2\sqrt{2}\pi d}\sqrt{\sum_{i=1}^{2}\arctan^2[\tilde{A}_i(x,y) - \tilde{A}_{bgi}(x,y) - \tilde{A}_{\mathrm{cor}i}]},$$
$$\theta(x,y) = \arctan\left(\frac{\arctan[\tilde{A}_2(x,y) - \tilde{A}_{bg2}(x,y) - \tilde{A}_{\mathrm{cor2}}]}{\arctan[\tilde{A}_1(x,y) - \tilde{A}_{bg1}(x,y) - \tilde{A}_{\mathrm{cor1}}]}\right) - \frac{\pi}{4}. \quad (25)$$

The formulas (24) and (25) allow us to receive gradient images, which are corrected on the background retardance, illumination intensity fluctuations, LC retardance variations, and systematic errors.

After correction of the gradient vector field, we can compute an enhanced regular DIC image with any shear direction, shear amount, and bias retardation using formula (5) with zero offset term. The computed image will be a pure phase gradient image with less noise and without deterioration caused by absorption, illumination nonuniformity, and light scattering.

F. Computation of Optical Path Image

The obtained optical path gradient vector field allows us to compute the corresponding two-dimensional scalar field, the optical path, by using numerical integration. The gradient field is a conservative vector field; the computed optical path depends only on the endpoints of that integral, not the particular integration route taken.

Many computation techniques could be employed for determining the optical path, for instance, line integration [16,36], the iterative method [37], various modifications of Fourier integration [11–15,20,38,39], the extended Fried algorithm [40], etc. In principle, any of these methods could be employed with use of our OI-DIC microscope. We shall not compare them in this current publication because it expands its size substantially. So it will be done in a separate article.

We use the optical path computation, developed by Biggs (KB Imaging Solution LLC, Loomis, California), which is based on iterative deconvolution approach. This technique employs the same principles as deconvolution techniques normally used to remove out-of-focus haze [41–43].

4. EXPERIMENTAL VERIFICATION

The first experimental setup in the transmitted mode, which is shown in Fig. 1, was implemented on an upright microscope Olympus BX-61 (Olympus America, Center Valley, Pennsylvania). The beam-shearing assemblies employed two pairs of regular DIC prisms in their original mounts and 2.2 mm thick liquid-crystal 90° polarization rotators in custom-made 7 mm thick holders. The axial displacement of the outside prism **DIC4** in the imaging path was 32 mm up, and the axial displacement of the outside prism **DIC1** in the illumination path was 16 mm down. The internal prisms **DIC2** and **DIC3** were placed in the originally designed positions. We made a single displacement compensator, which corrects

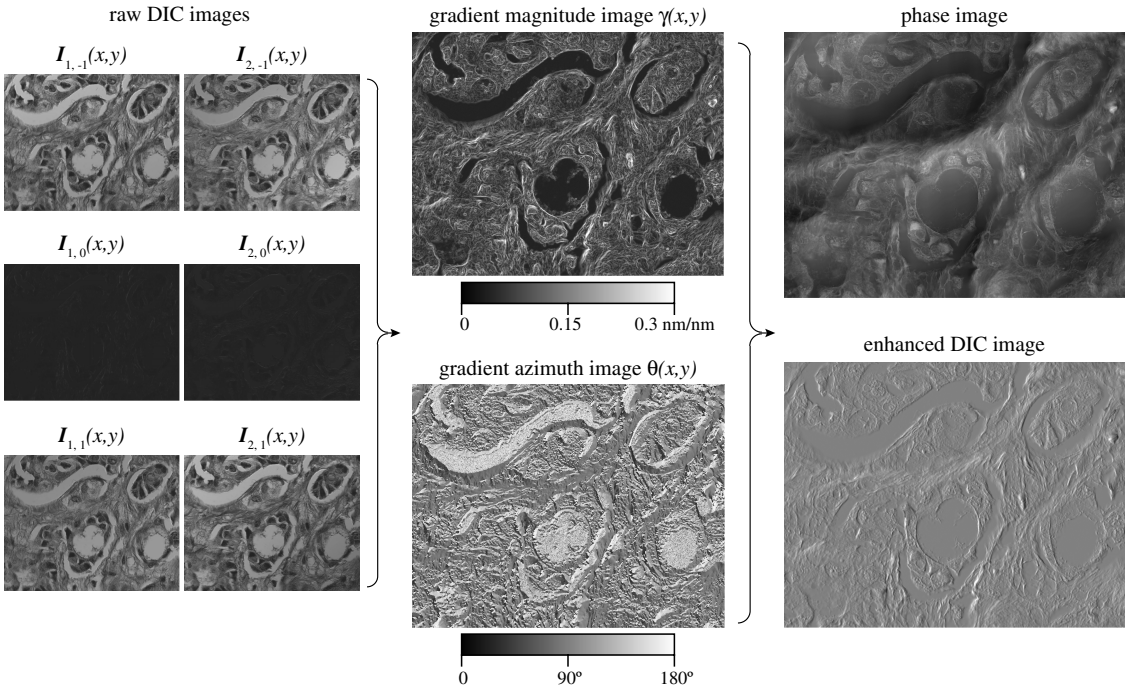

Fig. 4. OI-DIC images of the hematoxylin-eosin (H&E) stained breast cancer tissue sample.

misalignment in the interfering beams caused by displacements of both outside prisms. The LC optics was made by Boulder Vision Optics (Boulder, Colorado). The images were captured by a monochromatic CCD camera Infinity 3-1M (Lumenera, Canada). Using Matlab (The MathWorks, Inc., Natick, Massachusetts), we developed software for setup control and image processing.

Figure 4 shows OI-DIC images of the hematoxylin-eosin (H&E) stained breast cancer tissue sample, which contains collagenous stroma collagen surrounding the nests of cancer cells. The pictures were taken using a 40x/0.75P UPlanFL objective lens and a 546/40 nm bandpath filter. The picture size is 186 μm × 145 μm. We employed two crossed high-resolution DIC prisms U-DICTHR in the top beam-shearing assembly. According to Table 1, the shear distance of a single prism equals 0.18 μm. Then the shear distance of the crossed prism pair is 0.25 μm (0.18 μm multiplied by $\sqrt{2}$). The bias modulation amplitude was 0.15λ.

Six raw DIC images $\boldsymbol{I}_{i,j}(x,y)$ are shown on the left, where $i=1$ and $i=2$ correspond to the X and Y shear directions, respectively. Notations $j=-1$, 0, 1 conform to bias -0.15λ, 0 or 0.15λ. All DIC images were captured within 1 s. In white light the specimen is mostly red. If there is a green filter in the optical path then many specimen structures become dark due to significant absorption in the green–blue spectral region. So the shadow-cast DIC features are hardly visible. But they are present, and the computer processing produces quantitative gradient magnitude and azimuth maps (shown in the center). Further computation allows us to receive the phase image and regular DIC picture with drastically improved clarity. The enhanced DIC image could be computed with any shear direction and amount without the need to rotate either specimen or DIC prisms. The shown enhanced DIC image was computed with the horizontal shear direction, for instance. It could be compared with a regular DIC image with the same shear direction, which is displayed on the top left.

Figure 5 shows an example of the phase OI-DIC image of a live crane fly spermatocyte during metaphase of meiosis I taken with a Olympus UPlanFl 100x/1.30 oil immersion objective lens and a 546/30 nm interference filter. The image size is 68 μm × 68 μm. The image acquisition and processing took about 1 s each. The three autosomal bivalent chromosomes are in sharp focus at the spindle equator, along with one of the X–Y sex univalents, which is located on the right. The tubular distribution of mitochondria surrounding the spindle is clearly evident. Both polar flagella in the lower centrosome are in focus, appearing as a letter "L" lying on its side. The experiment was done together with Prof. LaFountain

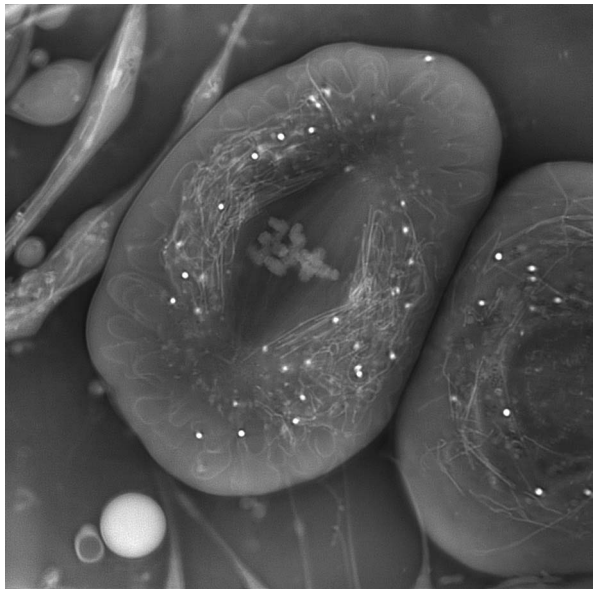

Fig. 5. Crane fly spermatocyte (full metaphase of meiosis-I). OI-DIC phase image; brightness is linearly proportional to refractive index.

(State University of New York, Buffalo, New York). The phase image was computed by Dr. Biggs (KB Imaging Solution LLC, Loomis, California), employing iterative deconvolution approach mentioned above.

5. CONCLUSION

Here we propose a quantitative OI-DIC microscope with high-speed switching shear direction and bias modulation. The microscope does not require mechanically rotating the specimen or the prisms. Therefore there is no image misalignment. All components do not require a special design and are available on the market. We proposed techniques for measuring the parameters of DIC prisms and calibrating the bias. Two sets of raw DIC images at the orthogonal shear directions are captured and processed within 1 s. Then the quantitative image of the optical path gradient distribution within a thin optical section is computed. The obtained data are also used to calculate the quantitative distribution of the optical phase, which represents refractive index gradient or height distribution. It is possible to generate back the enhanced regular DIC images with any desired shear direction.

APPENDIX A: MEASURING SHEAR DISTANCE

Shear amount (distance) is the critical parameter of a DIC microscope that determines its contrast, sensitivity, resolution, and optical section depth. Another issue with DIC microscopy is that, to derive quantitative information, one must know the amount of image shear. Generally, however, microscope manufacturers do not make that information available. As a result, one must measure this parameter. van Munster *et al.* [38] determined the lateral shift by measuring the distance between the center of the bright spot and the center of the dark spot in an image of a submicroscopic transparent latex sphere with bias set at $\pi/2$. Mehta and Sheppard [44] measured shear by studying the intensity distribution in the back focal plane of the microscope objective lens. Müller *et al.* [45] used a combination of fluorescence correlation spectroscopy and dynamic light scattering to determine shear. Duncan *et al.* [46] described a measurement setup using a standard optical wedge.

The below-described technique for determining shear distance is faster and more accurate than mentioned. We measure a shear angle and then compute the shear amount employing formula (1), as explained at the end of this section.

In order to find the shear angle of the DIC prism, we do not need to know how the passing beam is transformed inside the prism. The DIC prism splits an incident monochromatic plane wave into two orthogonally polarized plane waves with slightly different direction of their wavefronts. Figure 6 illustrates splitting the incident linearly polarized beam into two separate output beams with shear angle ε. Here the shear plane is parallel to the X axis. As one can see from the picture, the shear angle ε (in radians) equals the derivative of the optical path difference (bias) Λ with respect to the coordinate x:

$$\varepsilon = \frac{d\Lambda}{dx}. \tag{A1}$$

The optical path difference Λ is connected with retardance δ, written in degrees, and wavelength λ in a simple way:

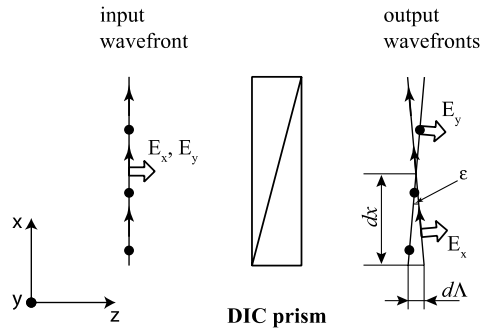

Fig. 6. Angular splitting the incident beam with two orthogonal polarization components E_x and E_y by a DIC prism into two output beams with shear angle ε.

$$\Lambda = \frac{\delta}{360^\circ}\lambda. \tag{A2}$$

Thus, the shear angle could be found by measuring a derivative of the retardance with respect to the coordinate along the shear direction:

$$\varepsilon = \frac{\lambda}{360^\circ}\frac{d\delta}{dx}. \tag{A3}$$

Retardance can be determined with a number of various techniques. In particular, one could employ the return-path compensation method, which we proposed in 1986 [47–49]. This simple technique is similar to the Senarmont compensator [50]. Because of superposition of the probe and reverse beams, the return-path arrangement has the following advantages: (i) owing to a double pass of a beam through a specimen under investigation, the sensitivity threshold is decreased by factor of two; (ii) the same optical elements are utilized twice, in the direct and the reverse beams. This makes the measurement setup less expensive considerably, which is very important, because one high-quality optical polarization element could cost several thousands dollars.

The schematic of the return-path setup is shown in Fig. 7. The device operates as follows. A laser radiates the collimated narrow beam, which is unpolarized or circularly polarized. The beam passes sequentially through a small hole in a screen, a Glan–Thompson polarization beam splitter, a quarter-wave plate (QWP), and a DIC prism. The DIC prism under investigation is placed on a linear stage with a Vernier micrometer. The stage allows us to move the prism in the horizontal direction. The beam passes through the QWP and the DIC prism two times, being reflected from a mirror. The beam splitter deflects the orthogonal polarization component toward a screen. The minimum intensity of the deflected laser beam was visually determined by observing the laser spot brightness on the screen. It is also possible to use a photodiode (PD) to measure the beam intensity. The intensity of the radiation flux of the deflected orthogonal component I' is described by the following formula [51]:

$$I' = I\{\cos\,\delta\,\sin\,2(\zeta-\chi) - \sin\,\delta\,\cos\,2(\zeta-\chi)\sin\,2(\zeta-\psi)\}^2, \tag{A4}$$

where I is the probing beam intensity, δ is retardance of the DIC prism, ψ is angular orientation of its shear plane, χ is the

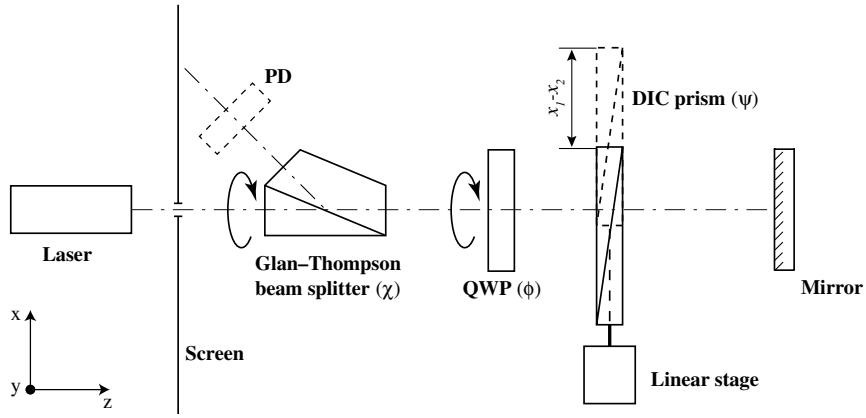

Fig. 7. Setup for measuring the shear angle of a DIC prism employing the return-path birefringence compensator.

orientation of the principal plane of the polarization beam splitter, and ζ is the orientation of the fast axis of the QWP.

The measuring procedure of the retardance derivative consists of the following steps. Before placing the DIC prism under investigation in the setup, we look at this prism between the crossed polarizers. The shear plane would be perpendicular to the observed color fringes or/and the black fringe. Let us note the shear plane orientation.

Next we take out the QWP from the setup, and put the DIC prism into the optical path. In this case, the beam intensity on the screen is determined by the following expression:

$$I' = I \sin^2 \delta \sin^2 2(\chi - \psi). \tag{A5}$$

By rotating the polarization beam splitter from 0° to 180°, we achieve two extinctions of the laser spot on the screen. These extinctions differ by 90°. One of the extinctions occurs when the beam splitter transmission axis is parallel to the shear plane of the DIC prism, which we noted. In this case the beam splitter angular scale χ points precisely to the shear plane orientation ψ.

After that we place the QWP into the optical path. The fast axis of the QWP has to make an angle 45° with the shear plane orientation, i.e., $\zeta = \psi + 45°$. The beam splitter also has to be rotated by 45°. In this case, $\chi_0 = \psi + 45°$. Thus, the QWP's fast axis is parallel to the beam splitter transmission axis. The laser spot on the screen becomes bright. Using formula (A4) we could derive the following equation, which describes the spot's intensity:

$$I' = I \sin^2(\delta - 2(\chi - \chi_0)). \tag{A6}$$

Rotating the beam splitter allows us to extinguish the spot on the screen. The DIC prism retardance δ in a point of the laser beam incidence is determined by the simple formula

$$\delta = 2(\chi - \chi_0), \tag{A7}$$

where χ is the orientation angle of the beam splitter.

Using a linear stage, we move the DIC prism in the horizontal direction and measure retardances δ_1 and δ_2 in two points x_1 and x_2. The retardance derivative along the shear direction X could be found by the following formula:

$$\frac{d\delta}{dx} = \frac{\delta_1 - \delta_2}{(x_1 - x_2)\cos\psi} = \frac{2(\chi_1 - \chi_2)}{(x_1 - x_2)\cos\psi}. \tag{A8}$$

Then we compute the shear angle (in radians):

$$\varepsilon = \frac{\lambda}{180°} \frac{(\chi_1 - \chi_2)}{(x_1 - x_2)\cos\psi}. \tag{A9}$$

Instead of finding retardance values in two points only, we can measure the dependence of the analyzer angle χ on the laser beam position x and use its derivative in the formula above:

$$\varepsilon = \frac{\lambda}{180°} \frac{1}{\cos\psi} \frac{d\chi(x)}{dx}. \tag{A10}$$

In the described setup we utilized a generic green laser pointer with wavelength 532 nm, beam splitting Glan–Thompson polarizer MSBTS-10-45 (Karl Lambrecht, Chicago, Illinois, http://www.klccgo.com), and precision achromatic QWP AQ-100-0545 (Meadowlark, Frederick, Colorado, http://www.meadowlark.com). Because the beam of our laser pointer has a significant linearly polarized component, we placed a generic circular polarizer for a digital single-lens reflex (SLR) camera between the pointer and the screen. In particular we employed a Tiffen circular polarizer 52HTCP (www.tiffen.com).

The measurement procedure could be simplified using a custom-built assembly with a rotatable polarization beam splitter and QWP [48]. This approach would not require taking out and putting in the QWP.

Table 1 summarizes some results of the shear angle measurements of various DIC prisms currently manufactured by Olympus (Tokyo, Japan, http://www.olympus.com). The high-resolution DIC prism **U-DICTHR** has the smallest shear angle. The prism enables observations with high resolution but less glare even for thick specimen used in developmental and genetic research, such as finely structured diatoms, embryos, zebrafish, and *C*. elegans. The all-round prism **U-DICT** with the intermediate shear angle is suitable for observing a wide range of general specimens, such as tissue. High-contrast DIC prism **U-DICTHC** has the largest shear angle. Using this prism high contrast can be obtained even in high magnification observations of thin specimens, such as culture cells.

According to our measurement the shear angle of the all-round DIC prism is double that of the high-resolution prism

and half that of the high-contrast prism. Therefore some setups with different objective lenses and the same condenser lens could employ the same condenser DIC prism. The following microscope configurations have interchangeable condenser DIC prisms:

- U-DICTHR prism & 10x objective, U-DICT prism & 20x objective, U-DICTHC prism & 40x objective;
- U-DICT prism & 10x objective, U-DICTHC prism & 20x objective;
- U-DICTHR prism & 20x objective, U-DICT prism & 40x objective;
- U-DICTHR prism & 30x objective, U-DICT prism & 60x objective;
- U-DICT prism & 30x objective, U-DICTHC prism & 60x objective.

For example, condenser DIC prism U-DIC40, which is designed for a 40x objective lens and all-round DIC prism U-DICT, could be also used with a 20x lens and high-resolution DIC prism U-DICTHR. It is interchangeable with condenser prism U-DICT20HR. Condenser prisms U-DIC20 and U-DIC40HC could be also mutually replaced.

We also found that the focal distance of the dry top condenser lens is double the oil top condenser lens. Hence, the condenser prism designed for the oil condenser would work for the dry condenser and the one-step-lower-resolution objective prism. On the other hand, the condenser prism designed for the dry condenser could be paired with the oil condenser and the one-step-higher-resolution objective prism. For instance, the dry condenser DIC prism U-DIC60HC, which is designed to work with the 60x objective lens and high-contrast prism U-DICTHC, would also work with the oil condenser and all-round prism U-DICT. So, prism U-DIC60HC is interchangeable with prism U-ODICT60. Then it is also could work instead of U-ODIC30HR, as mentioned earlier. Another example of an interchangeable pair of prisms is U-DIC100 and U-ODIC100HR. The first prism is designed for the dry top condenser lens, 100x oil objective and U-DICT prism. The second prism is intended for the oil top condenser lens, 100x oil objective and U-DICTHR prism.

Table 1 shows the corresponding computed shear distance d in the object plane and the ratio of the shear distance to the Airy disk radius d/r_{Airy}. For the calculation we used standardized reference focal lengths of the tube lenses L_t for the infinity-focused objective lens, which are adopted by several microscope manufacturers:

$$d = \varepsilon \frac{L_t}{M}, \tag{A11}$$

where M is objective lens magnification. In particular, the reference focal length L_t is 180 mm for Olympus, 164.5 mm for Zeiss, and 200 mm for Nikon and Leica microscopes [6].

The radius of Airy disk r_{Airy} is determined by the following equation [6]:

$$r_{\text{Airy}} = 0.61 \frac{\lambda}{\text{NA}}, \tag{A12}$$

where NA is the objective lens NA.

The above data are shown for the green light ($\lambda = 532$ nm). The shear angle was about 4% less for the red light ($\lambda = 641$ nm).

We have measured parameters of Olympus DIC prism **U-DICTH**, which was manufactured in previous years. Its shear angle is the same as that of the prism **U-DICTHR**. Mehta and Sheppard [44] found the angular shear 74 μrad for the **U-DICTS** prism at wavelength 550 nm. This shear corresponds exactly to our result for the **U-DICT** prism. Our other results indicate that shear angles of Nikon **60x I** and Zeiss **PA63x/1.40III** DIC sliders are 76 and 71 μrad, respectively. According to formula (A11), the Nikon slider and 60x objective lens create the shear distance 0.25 μm, and the Zeiss slider and 63x objective lens introduce shear 0.18 μm.

APPENDIX B: CALIBRATION OF LC VARIABLE RETARDER FOR BIAS MODULATION

Another parameter, which has to be quantified, is a bias amount introduced by the phase shifter. Any method for measuring retardance could be used to find a dependence of bias on the applied voltage. For example, one could employ the return-path compensation method, which we described in Appendix A. However, all calibration methods would require taking the phase shifter out of a microscope and placing it into a separate measuring setup. But, on the other hand, a phase shift of the LC variable retarder depends on the temperature, wavelength, set of incidence angles of the passing rays, etc. Therefore it would be convenient to calibrate the LC variable retarder directly in the OI-DIC microscope (Figs. 1 and 2) in order to avoid mismatch between the calibration and actual data.

For measuring the dependence of the bias on the applied voltage, we could use preliminary calibrated DIC prisms. In a transmitted DIC microscope the total optical path difference (bias) between two interfering beams is created by a pair of DIC prisms. One of them is located in the imaging part, and another in the illumination part. Each of the prisms introduces its own bias, which is not uniform and has a gradient. However, the prisms are placed and oriented in a way that they mutually compensate the bias gradient. Thus, the total bias distribution becomes even across the objective back focal plane. The bias can be changed by a lateral shifting of one of the DIC prisms along the bias gradient direction. As shown in Appendix A [formula (A1)], the unitless bias gradient equals the shear angle (in radians). We can write the linear equation for the current bias $\Lambda(x)$:

$$\Lambda(x) = \tilde{\Lambda} + \varepsilon(x - x_0), \tag{B1}$$

where x and x_0 are the current and initial positions of the prism, and $\tilde{\Lambda}$ is the initial bias. The shear angle ε can be found in Table 1, or it can be measured, as described in Appendix A.

Usually, the DIC prism is shifted by a translation screw. Then the bias variation could be determined using the pitch of a screw thread p and revolution number R in the following way:

$$\Lambda(R) = \tilde{\Lambda} + \varepsilon p R. \tag{B2}$$

For example, Olympus high-resolution DIC prism U-DICTHR has a translation screw with pitch 2.5 mm. The screw allows a

maximum of five rotations. According to Table 1, the prism shear angle is 40 μrad. Using Eq. (15) we receive the bias variation $\Lambda = 100$ nm per screw 360° turn and the total range of the bias change $\Lambda_{\text{tot}} = 500$ nm. General Olympus DIC prism U-DICT has a 3 mm screw pitch and a maximum of five rotations. Consequently its bias variation Λ is 225 nm per screw turn and the total bias range Λ_{tot} is 1125 nm.

Let us consider the OI-DIC microscope for the transmitted light (Fig. 1), for instance. Before calibration, the phase shifter and polarization rotators are removed from the microscope. An empty area of the specimen under investigation is placed in the center of the view field. The DIC prisms are adjusted for the maximal image darkness. This means the prisms introduce zero total bias. Then the phase shifter is put into place.

Because the polarizer and analyzer are crossed and their transmissial axes are oriented at 45° to the principal axes of the orthogonal DIC prisms, the beam intensity in the image central area $I(V_{\text{rms}})$ could be described by the following equation:

$$I(V_{\text{rms}}) = \tilde{I}\sin^2\left(\frac{\pi}{\lambda}(\Lambda_\Sigma + \Gamma(V_{\text{rms}}))\right) + I_c, \tag{B3}$$

where $\tilde{I}$ is the beam intensity after the polarizer; Λ_1, Λ_2, Λ_3, and Λ_4 are biases contributed by prisms DIC1, DIC2, DIC3, and DIC4, respectively; $\Lambda_\Sigma = \Lambda_1 - \Lambda_2 - \Lambda_3 + \Lambda_4$ is the combined bias introduced by all prisms; $\Gamma(V_{\text{rms}})$ is the bias created by the phase shifter; V_{rms} is the effective (rms) value of the applied voltage; and I_c corresponds to a constant offset of the intensity signal.

If the setup is adjusted for the maximal extinction, then biases Λ_1, Λ_2, Λ_3, and Λ_4 compensate each other and $\Lambda_\Sigma = 0$. Thus, in the initial state of the OI-DIC setup, a dependence of beam intensity $I_0(V_{\text{rms}})$ on the applied voltage is determined by the formula

$$I_0(V_{\text{rms}}) = \tilde{I}\sin^2\left(\frac{\pi}{\lambda}\Gamma(V_{\text{rms}})\right) + I_c. \tag{B4}$$

Next we move laterally one of the DIC prisms by the same distance by rotating the translation screw in the clockwise and counterclockwise directions. According to the linear equation (15), in these cases the prism bias will change by amount $\pm(\varepsilon pR)$. The correspondent dependences of the beam intensity $I_{-1}(V_{\text{rms}})$) and $I_1(V_{\text{rms}})$ are determined by the following equations:

$$I_{-1}(V_{\text{rms}}) = \tilde{I}\sin^2\left(\frac{\pi}{\lambda}(\Gamma(V_{\text{rms}}) - \varepsilon pR)\right) + I_c, \tag{B5}$$

$$I_1(V_{\text{rms}}) = \tilde{I}\sin^2\left(\frac{\pi}{\lambda}(\Gamma(V_{\text{rms}}) + \varepsilon pR)\right) + I_c. \tag{B6}$$

Using the measured beam intensities $I_0(V_{\text{rms}})$, $I_{-1}(V_{\text{rms}})$, and $I_1(V_{\text{rms}})$ we can obtain the phase shifter bias $\Gamma(V_{\text{rms}})$):

$$\Gamma(V_{\text{rms}}) = \frac{\lambda}{2\pi}\arctan\left[\frac{I_1(V_{\text{rms}}) - I_{-1}(V_{\text{rms}})}{I_1(V_{\text{rms}}) + I_{-1}(V_{\text{rms}}) - 2I_0(V_{\text{rms}})} \times \tan\left(\frac{\pi}{\lambda}\varepsilon pR\right)\right]. \tag{B7}$$

The bias computation formula (B7) yields values within a $[0, \lambda]$ interval. In other words, without further analysis, the bias measurement cannot distinguish a certain bias value, say $\Gamma_0, \Gamma_0 + \lambda$. It is said that the measurement yields wrapped bias information. However, using prior knowledge regarding the continuity of the bias variation, the obtained result can be numerically corrected to cover greater intervals, outside $[0, \lambda]$, by mathematical operation called phase unwrapping. Mathematically, the unwrapping operation essentially searches for 2π jumps in the signal and corrects them by adding the 2π values back to the signal. For example, Matlab has a very efficient and fast standard command called "unwrap."

In order to build the correct bias dependence, it is also necessary to take into account a type of LC cell, which is employed in the phase shifter. In particular, retardance of the conventional Freedericksz ECB cell decreases with applied voltage. The retardance is minimal and equals about 0.1λ at the highest voltage. In the case of a VA ECB cell, the retardance is minimal and equals zero when no voltage is applied.

Similarly, the bias calibration method would work for the reflected light OI-DIC setup (Fig. 2). Because each DIC prism is used twice, in the illumination and reflected beams, the bias introduced by lateral movement of the prism is doubled. Therefore formula (B7) for the reflected light OI-DIC has to be modified in the following way:

$$\Gamma(V_{\text{rms}}) = \frac{\lambda}{2\pi}\arctan\left[\frac{I_1(V_{\text{rms}}) - I_{-1}(V_{\text{rms}})}{I_1(V_{\text{rms}}) + I_{-1}(V_{\text{rms}}) - 2I_0(V_{\text{rms}})} \times \tan\left(\frac{2\pi}{\lambda}\varepsilon pR\right)\right]. \tag{B8}$$

ACKNOWLEDGMENTS

The author thanks David Biggs of KB Imaging Solution LLC (Loomis, California) for helpful discussions and for providing software for computing phase images, and Richard Langill of the Marine Biological Laboratory (Woods Hole, Massachusetts) for hardware development. We are also grateful to Shinya Inoué of the MBL, and to James LaFountain of the State University of New York (Buffalo, New York) for their encouragement and support. This publication was made possible by Grant No. R01-GM101701 from the National Institute of General Medical Sciences, National Institutes of Health. Its contents are solely the responsibility of the author and do not necessarily represent the official views of the National Institute of General Medical Sciences or the National Institutes of Health.

REFERENCES

1. F. H. Smith, "Interference microscope," U.S. patent 2,601,175 (August 5, 1947).
2. F. H. Smith, "Microscopic interferometry," Research **8**, 385–395 (1955).
3. G. Nomarski, "Interferential polarizing device for study of phase object," U.S. patent 2,924,142 (May 14, 1952).
4. R. D. Allen, G. B. David, and G. Nomarski, "The Zeiss-Nomarski differential equipment for transmitted light microscopy," Zeitschrift für Wissenschaftliche Mikroscopie und Mickroskopische Technik **69**, 193–221(1969).
5. S. Inoué, "Ultrathin optical sectioning and dynamic volume investigation with conventional light microscopy," in *Three-Dimensional Confocal Microscopy: Volume Investigation of*

Biological Systems, J. Stevens, ed. (Academic, 1994), pp. 397–419.
6. R. Oldenbourg and M. Shribak, "Microscopes," in *Geometrical and Physical Optics*, *Polarized Light*, *Components and Instruments*, M. Bass, ed., 3rd ed., Vol. **1** of Handbook of Optics (McGraw-Hill, 2010), pp. 28.1–28.62.
7. G. M. Holzwarth, S. C. Webb, D. J. Kubinski, and N. S. Allen, "Improving DIC microcopy with polarization modulation," J. Microsc. **188**, 249–254 (1997).
8. G. M. Holzwarth, D. B. Hill, and E. B. McLaughlin, "Polarization-modulated differential-interference contrast microscopy with a variable retarder," Appl. Opt. **39**, 6288–6294 (2000).
9. H. Ooki, Y. Iwasaki, and J. Iwasaki, "Differential interference contrast microscope with differential detection for optimizing image contrast," Appl. Opt. **35**, 2230–2234 (1996).
10. P. Hariharan and M. Roy, "Achromatic phase-shifting for two-wavelength phase-stepping interferometry," Opt. Commun. **126**, 220–222 (1996).
11. M. R. Arnison, K. G. Larkin, C. J. R. Sheppard, N. I. Smith, and C. J. Cogswell, "Linear phase imaging using differential interference contrast microscopy," J. Microsc. **214**, 7–12 (2004).
12. S. V. King, A. R. Libertun, C. Preza, and C. J. Cogswell, "Calibration of a phase-shifting DIC microscope for quantitative phase imaging," Proc. SPIE **6443**, 64430M (2007).
13. H. Ishiwata, M. Itoh, and T. Yatagai, "A new method of three-dimensional measurement by differential interference contrast microscope," Opt. Commun. **260**, 117–126 (2006).
14. H. Ishiwata, M. Itoh, and T. Yatagai, "A new analysis for extending the measurement range of the retardation-modulated differential interference contrast (RM-DIC) microscope," Opt. Commun. **281**, 1412–1423 (2008).
15. A. Noguchi, H. Ishiwata, M. Itoh, and T. Yatagai, "Optical sectioning in differential interference contrast microscopy," Opt. Commun. **282**, 3223–3230 (2009).
16. M. Shribak and S. Inoué, "Orientation-independent differential interference contrast microscopy," Appl. Opt. **45**, 460–469 (2006).
17. M. Shribak, "Orientation-independent differential interference contrast microscopy technique and device," U.S. patent 7,564,618 (December 17, 2003).
18. M. Shribak, "Orientation-independent differential interference contrast microscopy technique and device," U.S. patent 7,233,434 (December 17, 2003).
19. L. Fabre, Y. Inoue, T. Aoki, and S. Kawakami, "Differential interference contrast microscope using photonic crystals for phase imaging and three-dimensional shape reconstruction," Appl. Opt. **48**, 1347–1357 (2009).
20. C. Preza, D. L. Snyder, and J. A. Conchello, "Theoretical development and experimental evaluation of imaging models for differential-interference-contrast-microscopy," J. Opt. Soc. Am. A **16**, 2185–2199 (1999).
21. H. Hogan, "Getting the small picture," Photonics Spectra **37**(4), 58–64 (2003).
22. R. Danz and P. Gretscher, "C-DIC: a new microscopy method for rational study of phase structures in incident light arrangement," Thin Solid Films **462-463**, 257–262 (2004).
23. M. Robinson, J. Chen, and G. Sharp, *Polarization Engineering for LCD Projection* (Wiley, 2005).
24. R. A. Chipman, "Polarimetry," in *Geometrical and Physical Optics*, *Polarized Light*, *Components and Instruments*, M. Bass, ed., 3rd ed., Vol. **1** of Handbook of Optics (McGraw-Hill, 2010), pp. 15.1–15.46.
25. T. Scharf, *Polarized Light in Liquid Crystals and Polymers* (Wiley, 2007).
26. E. Lueder, *Liquid Crystal Displays: Addressing Schemes and Electro-Optical Effects* (Wiley, 2010).
27. S. Gauza and S.-T. Wu, "Liquid crystals," in *Atmospheric Optics*, *Modulators*, *Fiber Optics*, *X-Ray And Neutron Optics*, M. Bass, ed., 3rd ed., Vol. **5** of Handbook of Optics (McGraw-Hill, 2010), pp. 8.1–8.40.
28. E. D. Salmon and P. Tran, "High resolution video-enhanced differential-interference contrast (VE-DIC) light microscopy," Meth. Cell Biol. **56**, 153–184 (1998).
29. B. J. Schnapp, "View single microtubules by video light microscopy," Meth. Enzymol. **134**, 561–573 (1986).
30. M. Shribak, S. Inoué, and R. Oldenbourg, "Rectifiers for suppressing depolarization caused by differential transmission and phase shift in high NA lenses," Proc. SPIE **4481**, 163–174 (2001).
31. M. Shribak, S. Inoué, and R. Oldenbourg, "Polarization aberrations caused by differential transmission and phase shift in high NA lenses: theory, measurement and rectification," Opt. Eng. **41**, 943–954 (2002).
32. P. Hariharan, *Optical Interferometry*, 2nd ed. (Academic, 2003).
33. M. Shribak, Y. Otani, and T. Yoshizawa, "Autocollimation polarimeter for measuring two-dimensional distribution of birefringence," Opt. Spectrosc. **89**, 155–159 (2000).
34. M. Shribak and R. Oldenbourg, "Techniques for fast and sensitive measurements of two-dimensional birefringence distributions," Appl. Opt. **42**, 3009–3017 (2003).
35. M. Shribak, "Complete polarization state generator with one variable retarder and its application for fast and sensitive measuring of two-dimensional birefringence distribution," J. Opt. Soc. Am. A **28**, 410–419 (2011).
36. B. Heise, A. Sonnleitner, and E. P. Klement, "DIC image reconstruction on large cell scans," Microsc. Res. Tech. **66**, 312–320 (2005).
37. C. Preza, "Rotational-diversity phase estimation from differential-interference-contrast microscopy images," J. Opt. Soc. Am. A **17**, 415–424 (2000).
38. E. B. van Munster, L. J. van Vliet, and J. A. Aten, "Reconstruction of optical pathlength distributions from images obtained by a wide-field differential interference contrast microscope," J. Microsc. **188**, 149–157 (1997).
39. S.-K. Yu, T.-K. Liu, and S.-C. Lin, "Height measurement of transparent objects by adopting differential interference contrast technology," Appl. Opt. **49**, 2588–2596 (2010).
40. S. A. Prahl, A. Dayton, K. Juedes, E. J. Sanchez, R. P. Lopez, and D. D. Duncan, "Experimental validation of phase using Nomarski microscopy with an extended Fried algorithm," J. Opt. Soc. Am. A **29**, 2104–2109 (2012).
41. T. J. Holmes, S. Bhattacharyya, J. A. Cooper, D. Hanzel, V. Krishnamurthi, W. Lin, B. Roysam, D. H. Szarowski, and J. N. Turner, "Light microscopic images reconstructed by maximum likelihood deconvolution," in *Handbook of Biological Confocal Microscopy*, J. B. Pawley, ed. (Plenum, 1995) pp. 389–402.
42. D. Biggs and M. Andrews, "Acceleration of iterative image restoration algorithms," Appl. Opt. **36**, 1766–1775 (1997).
43. M. Shribak, J. LaFountain, D. Biggs, and S. Inoué, "Orientation-independent differential interference contrast microscopy and its combination with an orientation-independent polarization system," J. Biomed. Opt. **13**, 014011 (2008).
44. S. B. Mehta and C. J. R. Sheppard, "Sample-less calibration of the differential interference contrast microscope," Appl. Opt. **49**, 2954–2968 (2010).
45. C. B. Müller, K. Weiß, W. Richtering, A. Loman, and J. Enderlein, "Calibrating differential interference contrast microscopy with dual-focus fluorescence correlation spectroscopy," Opt. Express **16**, 4322–4329 (2008).
46. D. D. Duncan, D. G. Fischer, A. Dayton, and S. A. Prahl, "Quantitative Carré differential interference contrast microscopy to assess phase and amplitude," J. Opt. Soc. Am. A **28**, 1297–1306 (2011).
47. M. I. Shribak, "Device for measuring birefringence of reflecting optical data carrier," USSR patent 1,414,097 (March 17, 1986).
48. M. I. Shribak, "A compensation method for measuring birefringence," Sov. J. Opt. Technol. **60**, 546–549 (1993).
49. M. I. Shribak, "Autocollimating detectors of birefringence," Proc. SPIE **2782**, 805–813 (1996).
50. N. H. Hartshorne and A. Stuart, *Crystals and the Polarizing Microscope*, 4th ed. (Edward Arnold, 1970).
51. M. I. Shribak, "Polarization separation of the forward and reverse beams in the reading of reflective carriers of information," Sov. J. Opt. Technol. **53**, 389–391 (1986).